RESEARCH ARTICLE

NANO · MICRO small
www.small-journal.com

Brønsted–Lowry Acid-Based Aqueous Eutectic Electrolyte for Practical Zinc Batteries

Roza Bouchal, Ibrahim Al Kathemi, and Markus Antonietti**

Aqueous highly concentrated electrolytes (AHCEs) have recently emerged as an innovative strategy to enhance the cycling stability of aqueous Zinc (Zn) batteries (AZB). Particularly, thanks to high Zn Chloride ($ZnCl_2$) solubility in water, AHCEs based on $ZnCl_2$ feature remarkable Zn anode stability. However, due to their inherently acidic pH and Cl^- anion reactivity, these electrolytes face compatibility challenges with other battery components. Here, an aqueous eutectic electrolyte (AEE) based on Brønsted–Lowry concept is reported—allowing the usage of cheap and abundant salts, $ZnCl_2$, and sodium acetate (NaAc). The reported, pH buffered, AEE displays a higher coordination of water at an even lower salt concentration, by simply balancing the acceptor–donor H—bonding. This results in impressive improvement of electrolyte properties such as high electrochemical stability, high transport properties and low glass transition temperature. The developed AEE displays higher compatibility with vanadium oxide-based cathode with a 50% increase in capacity retention in comparison to sat. $ZnCl_2$. More importantly, the pH buffered AEE solves the incompatibility issues of $ZnCl_2$ toward commonly used aluminium (Al) current collector as well as cellulose separator. This work presents an efficient, simple, and low-cost strategy for the development of aqueous electrolytes for the practical application of Zn batteries.

1. Introduction

Zn batteries have been around since Daniell's invention of Cu—Zn battery in 1836. Primary (non-rechargeable) Zn batteries such as alkaline Zn–manganese, Zn–nickel, and Zn–silver oxide account for one-third of the world's battery market.[1,2] The Zn metal electrode is cheap (about USD 2 kg^{-1}), abundant, intrinsically safe, and can offer a high theoretical capacity (820 $mAh \cdot g^{-1}$) at low electrochemical potential (−0.762 V vs the standard hydrogen electrode (SHE)).[1,3] These advantages accelerated the development of rechargeable Zn batteries, which began with the discovery of the Zn intercalation cathodes. Today AZB, at the laboratory level, offers an energy density of ≈90 $Wh \cdot kg^{-1}$ at very low costs of ≈\$25 $kW \cdot h^{-1}$ – five times less than Li-ion batteries.[4,5] As a result, AZB is regarded as an excellent candidate for grid storage applications. Nonetheless, despite its numerous advantages, the use of Zn metal anode remains difficult. Due to dendrite formation, Zn corrosion, and a low plating/stripping efficiency in many standard systems, Zn metal suffers from several degradation processes during cycling, resulting in a still poor battery life and performance.[6,7]

The occurrence of water decomposition via the hydrogen evolution reaction (HER) is one of the main issues of Zn metal anode. In fact, parasitic HER competes with the Zn plating process during battery cycling.[8] The generation of a hydroxyl ion (OH^-) during water decomposition leads to the formation of $Zn(OH)_2$, which further converts to insoluble ZnO, which is electrochemically inactive.[9] To reduce the contribution of HER, AHCEs can be applied, with water being thermodynamically stabilized in the hydration shell of the ions.[10,11] The wide electrochemical stability window (ESW) of AHCEs improves considerably the cycling stability, particularly at low scan rates. AHCEs based on concentrated $ZnCl_2$ represent a promising group of electrolytes, showing a stable Zn plating stripping with relatively low overpotential.[13–17] Indeed, $ZnCl_2$ is one of the most soluble Zn salts in water and was previously used as a dendrite inhibitor to stabilise the Zn anode.[12] The high concentrations mitigate the activity of Cl^- by cation stabilization, thus allowing a higher ESW at both anodic and cathodic sides.[16] However, despite the mitigation of the activity of Cl^-, the stability of the cathode material can be altered resulting in low capacity retention.[16] More importantly, these electrolytes are very acidic and corrosive towards metals especially commonly used Al current collector, which restrict their application at the industrial level.[13,17] Another challenge of highly concentrated $ZnCl_2$ is its incompatibility towards cellulose, which is currently the best choice for truly sustainable batteries. Saturated $ZnCl_2$ in water is known to dissolve cellulose as $[ZnCl_4]^{2-}$ is rather acidic and breaks hydrogen bonds.[17–19]

Ac anion can serve as an effective buffering agent for elevating solution pH. Previously utilized in contexts such as ionic liquids and eutectic solvents, one example is ethyl-3-methylimidazolium Ac, which has been observed to exhibit greater basicity than water

R. Bouchal, I. Al Kathemi, M. Antonietti
Max Planck Institute of Colloids and Interfaces
Am Mühlenberg 1, 14476 Potsdam, Germany
E-mail: roza.bouchal@mpikg.mpg.de; markus.antonietti@mpikg.mpg.de

The ORCID identification number(s) for the author(s) of this article can be found under https://doi.org/10.1002/smll.202309556

DOI: 10.1002/smll.202309556

itself.[20] M. Yang et al. recently reported Zn Ac mixed with $ZnCl_2$ to prepare highly concentrated eutectic electrolytes. Although the aim of their study was not related to the benefit of Ac as a buffer and increasing the pH, they showed the ability of Ac to interact with Zn and water to reduce the HER and dendrite formation. However, to obtain a homogenous mixture, the resulting eutectic electrolyte is extremely viscous (40 000 mPa·s) with poor ionic conductivity of $1 mS \cdot cm^{-2}$, resulting in low rate capabilities.[21] Therefore, for efficient development of practical aqueous electrolytes, the following criteria should be considered: i) high transport properties including high ionic conductivity, especially Zn conductivity reflected by high transference number, ii) low glass transition temperature, the electrolyte should stay liquid during low winter temperatures, iii) compatibility towards the battery components and iv) safety, sustainability and environment-friendly materials.

Here, we report an AEE based on Brønsted–Lowry concept by simply mixing a Lewis acid ($ZnCl_2$) with a weak Brønsted base (NaAc), we are able to change the electrolyte parameters to a large extent. This simple strategy aims to obtain a well optimized $ZnCl_2$/NaAc/water ratio to simultaneously increase the pH of the electrolyte, the ionic conductivity and the ESW. Furthermore, the optimized ratio was tested in a full battery cell showing an improved stability of both Zn anode and vanadium oxide-based cathode. More importantly, the obtained AEE features improved properties – allowing an impressive reduction of Al corrosion while stabilizing the cellulose separator. This work proposes a simple and effective strategy for electrolyte development for the future commercialization of AZB.

2. Results and Discussion

2.1. Design of AEE

Aqueous $ZnCl_2$ solutions are acidic and well known for their corrosiveness toward metals.[17] In aqueous solutions, Zn^{2+} cations are solvated by dipolar water molecules, which gives rise to aqua ions $(Zn(OH_2)_6)^{2+}$.[22] The metal ion acts as a Lewis acid and interacts with one pair of water, an amphoter, which then creates an acidic proton. Thus, the cation–solvent interaction has a profound effect on the pH of the resultant solutions.[9] On the other hand, anions can have a similar effect on the water, polarizing the H-bond as a Lewis base and creating Brønsted alkalinity.

Our strategy to simultaneously keep the high Zn salt concentration while increasing the solution pH is to make AEEs with the highly soluble $ZnCl_2$ and NaAc. For that, $(ZnCl_2)_x(NaAc)_{1-x}/(H_2O)_n$ mixtures at saturation were prepared; x is the salt mixing mole ratio (x = 0, 0.2, 0.4, 0.5, 0.6, 0.8, 1) and n is the salt/H_2O molar ratio (see Table S1, Supporting Information). The sat. $ZnCl_2$/NaAc mixtures were compared with saturated NaAc (sat. NaAc) and $ZnCl_2$ (sat. $ZnCl_2$) hypersaline solutions corresponding to $x = 0$ and $x = 1$, respectively. **Figure 1a** shows the miscibility limits of mixed salts in pure water at room temperature. Except for sat. $ZnCl_2$ with a maximum concentration of 31.2 m, the 0.6 and 0.5 electrolytes allow the highest salt concentrations corresponding to 20.8 and 18.5 m, respectively. All the electrolyte ratios display a homogenous and transparent liquid. As shown in Figure 1b, the electrolyte pH value steadily increases with NaAc concentration, from pH 2 in sat. $ZnCl_2$ to pH6 in the $x = 0.2$ electrolyte. Other Ac salts (lithium and ZnAc) were also mixed with $ZnCl_2$ in water at room temperature. The ZnAc was not possible to mix with $ZnCl_2$ with low water content. The electrolytes with lithium acetate were homogenous but viscous and the pH of the resulting solutions was not increased as in the presence of NaAc (data not reported here). This confirms the role of both Ac anion and counter cation in increasing the pH of the saline solution.

2.2. Physico-Chemical Characterization

Differential scanning calorimetry (DSC) was performed to characterize the thermal properties of the associated solutions. Figure 1c shows the heat change of the different electrolytes compared with sat. $ZnCl_2$ and sat. NaAc in the temperature range from –150 to 45 °C. All the samples show various solid–liquid transitions including glass transition, cold crystallization and ice melting; summarized in Table S2 (Supporting Information). In accordance with the literature, sat. $ZnCl_2$ sample shows a low solid-liquid transition temperature (T_t) at –63.4 °C, a cold crystallization at –6 °C and a melting point at 15.5 °C. Electrolytes with the higher $ZnCl_2$ content ($x = 0.8$ and $x = 0.6$) show also this high melting onset point of 0 and 4 °C, respectively. The cold crystallization observed in both sat. $ZnCl_2$ and $x = 0.8$ electrolyte refers to the crystallization from a glassy/amorphous phase suggesting the presence of crystals. On the other hand, $x = 0.5$ and $x = 0.4$ electrolytes demonstrate only a glass transition temperature at –76.9 and –84 °C, respectively, showing a wide range of liquid phase. Here, the ion and cation disorder and interaction suppress crystallization. Finally, the electrolyte with high NaAc concentration ($x = 0.2$) and sat. NaAc both show a low solid-liquid transition temperature. $x = 0.2$ electrolyte shows two glass transitions at –89.9 and –46.5 °C indicating a phase separation.[23] Sat. NaAc, on the other, hand possesses a glass transition at –94.4 °C, cold crystallization at –63.9 °C and ice melting at –50 °C. From these results, it is clear that the presence of NaAc decreases all transition temperatures of the electrolyte as shown in Figure 1d. The results show that Brønsted–Lowry acid-based AEEs can be obtained at optimized $ZnCl_2$/NaAc ratios of $x = 0.5$ and $x = 0.4$, exhibiting low T_t and thus a wide liquid phase of the electrolyte.

The concentration-dependence of viscosity (η) and ionic conductivity (σ) at 20 °C of the different electrolytes are shown in Figure 1e. Overall, the presence of NaAc brings a higher electrolyte conductivity and lower viscosity. For instance, the viscosity of $x = 0.2$ and $x = 0.5$ AEE are 11 and 40 mPa·s, respectively, in comparison to 585 mPa·s in sat. $ZnCl_2$. The latter solution was left overnight to absorb humidity from the air, and the viscosity dropped to only 350 mPa s, which is still higher than $ZnCl_2$/NaAc mixtures. The ionic conductivity of $x = 0.5$ AEE electrolyte at 20 °C is 21.5 $mS \cdot cm^{-1}$ compared to 4.8 $mS \cdot cm^{-1}$ in sat. $ZnCl_2$, which is also higher than the commercial nonaqueous electrolytes (10 $mS \cdot cm^{-1}$ at 20 °C) used in Li-ion batteries.[24]

The temperature dependence of the viscosity and the ionic conductivity of the different electrolytes were determined to study the temperature-transport properties relationship and the ionicity. The Figure S1a,b (Supporting Information) display the Arrhenius plot of the ionic conductivity and viscosity, respectively, which indicate a non-linear correlation to ($1/T$). Therefore, the

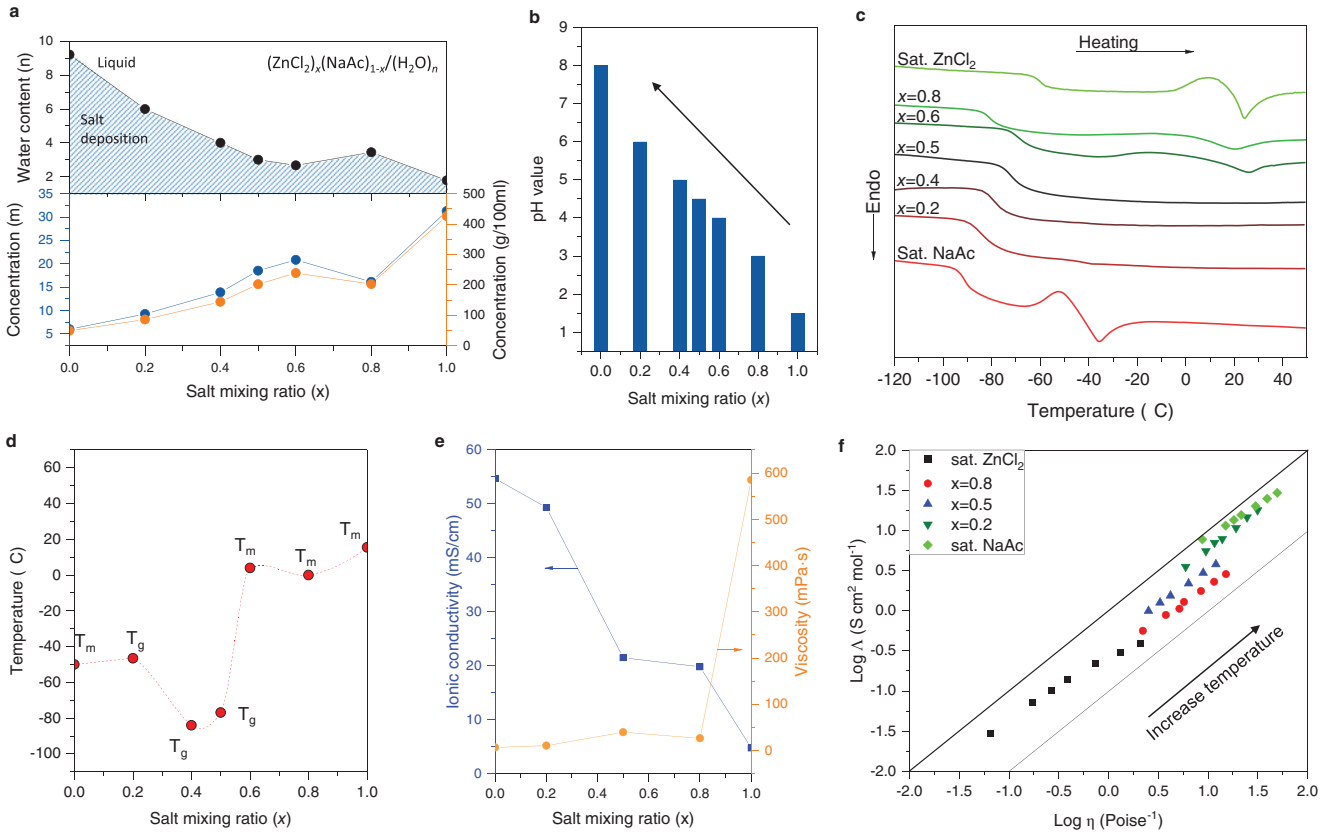

Figure 1. Preparation of AEEs and their physicochemical properties. a) Liquidus line of $(ZnCl_2)_x(NaAc)_{1-x}$ salt-water mixtures obtained by connecting saturation points (filled circles) experimentally obtained through the gradual addition of water to $(ZnCl_2)_x(NaAc)_{1-x}$ salts with the given values of x. The region above the liquidus line represents a stable liquid phase of fully miscible salts and water. b) pH values of the sat. $ZnCl_2$/NaAc mixtures compared with sat. $ZnCl_2$ and sat. NaAc solutions. c) DSC results obtained from −150 to 45 °C at a heating rate of 10 °C·min^{-1}. d) Solid-liquid transition temperature from DSC tests. T_g = glass transition temperature and T_m = melting temperature. e) Ionic conductivity versus the salt mixing ratio (x) compared to the viscosity values obtained at 20 °C. f) Walden plot in the temperature range of 10–60 °C. Λ, is the equivalent conductivity and η^{-1} is the fluidity. The ideal line passing in the middle corresponds to the aqueous 0.01 M KCl solution.

relationship of ion conductivity and viscosity on the temperature (T) was fitted using the Vogel–Fulcher–Tammann (VFT) equation:

$$\sigma = \sigma_0 \exp\left(-\frac{B_\sigma}{(T - T_{0\sigma})}\right) \quad (1)$$

$$\eta = \eta_0 \exp\left(\frac{B_\eta}{(T - T_{0\eta})}\right) \quad (2)$$

where the fitting parameters: σ_0 and η_0, are pre-exponential factors, B_i is a factor related to the activation/pseudo-activation energy, and T_{0i} is the dynamic glass transition temperature. The activation energy for ion transport and viscous flow, E_σ and E_η, can be extracted via $B_i = E_i/R$ where R is the gas constant. The fitted parameters are summarized in Tables S3 and S4 (Supporting Information).

The obtained dynamic glass temperatures from both ionic conductivity ($T_{0\sigma}$) and viscosity ($T_{0\eta}$) only display slight convergence. For sat. $ZnCl_2$ both $T_{0\eta}$ and $T_{0\sigma}$ are lower than T_g by 7 to 13 °C comparable to ionic liquids which are typically 10 to 50 °C inferior to the T_g.[25,26] However, the mixed $ZnCl_2$/NaAc and especially sat. NaAc, $T_{0\eta}$ is higher than T_g. The same observation for $T_{0\sigma}$ except in $x = 0.5$ AEE which is slightly lower by 3 °C. Nevertheless, the $ZnCl_2$/NaAc mixtures, particularly $x = 0.5$ AEE, display a lower difference between T_0 and T_g (see Tables S3 and S4, Supporting Information). The results suggest a greater fragility in the eutectic electrolyte, leading to a higher rate of change in transport properties and relaxation dynamics around T_g.[26,27] The apparent activation energy of ionic motion and viscous flow are similar with all electrolytes except sat. $ZnCl_2$. Moreover, the obtained E_σ are in agreement with LiTFSI/H_2O[27] and $Li(TFSI)_{0.75}(OTf)_{0.25}$[28] water-in-salt electrolytes (0.04 – 0.09 eV). Overall, the consistency of the fitted T_{0i} and E_i drove from both σ and η in the $ZnCl_2$/NaAc electrolytes, indicates a low degree of decoupling between σ and η or a high degree of assistance provided by the solvent molecules to the ion transport.[29] Furthermore, the Walden plot is presented in Figure 1f to identify the transport properties (η and σ) relationship and to assess the ionicity. The viscosity-molar conductivity relationship was determined from the logarithmic form of the Walden rule reported by Yang et al.[13] (see supporting information for the detailed calculation).

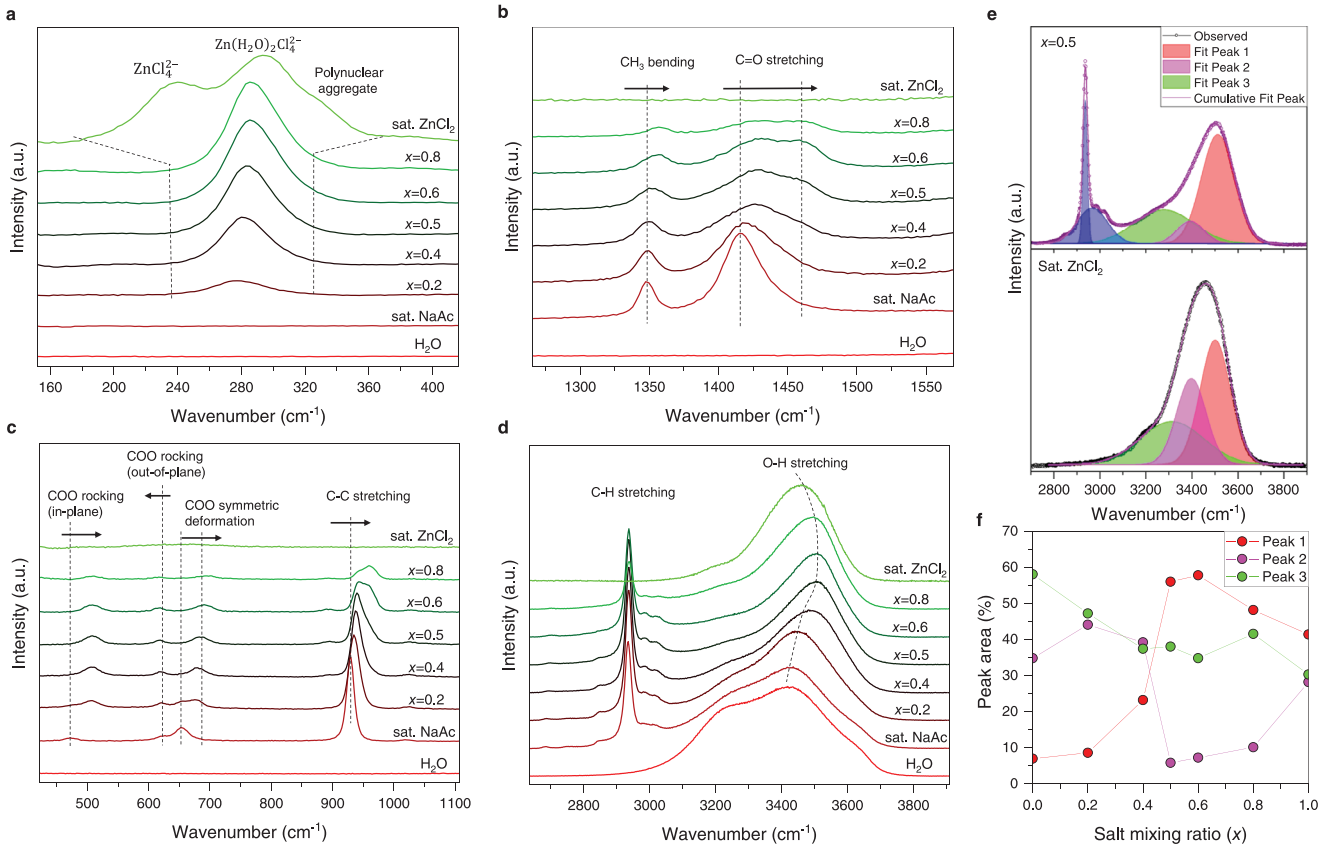

Figure 2. Structural characterization of $ZnCl_2$/NaAc mixtures. a–c) Raman spectra of $ZnCl_2$/NaAc mixtures at different compared with sat. $ZnCl_2$, sat. NaAc solutions and pure water. a) corresponds to the Zn solvation region. b,c) Ac anion corresponding bands region. d) Raman bands of O—H stretching modes of water molecules.

All the electrolytes are located close to the ideal line and are considered good electrolytes with an ionicity ≥90%. Clearly, the addition of NaAc increases steadily the ionicity of the $ZnCl_2$/NaAc mixtures as sat. NaAc features the highest ionicity close to the KCl line. The sat. $ZnCl_2$, however, exhibits a lower level of ionicity, which aligns with the findings reported by Yang et al.[13] This observation is further supported by the Raman spectroscopy results discussed in the following section, suggesting the presence of ion pairing in the sat. $ZnCl_2$. The eutectic electrolyte $x = 0.5$ AEE shows a much-improved ionicity in comparison to both $x = 0.8$ and sat. $ZnCl_2$. Although $x = 0.8$ has a lower salt concentration of 16.1m compared to $x = 0.5$ AEE with 18.5 m. These results indicate that the ratio between $ZnCl_2$ and NaAc plays an important role in the transport properties rather than the total salt concentration. Overall, our results are in accordance with the previously reported AHCEs as summarized in the reported review by Han et al.[30]

Raman spectroscopy was performed to understand the effect of $ZnCl_2$/NaAc ratio on the electrolyte structure, the evolution of H-bonds and cation-anion interactions. In **Figure 2**, the spectra of the different electrolytes were compared with sat. $ZnCl_2$, sat. NaAc, and H_2O solutions. The solvation configuration of Zn^{2+} in various electrolytes can be followed in the region of 200–450 cm^{-1} as shown in Figure 2a. Pure water and sat. NaAc electrolyte show no peaks around this region. A new peak at 278 cm^{-1} is observed upon the introduction of $ZnCl_2$, which keeps increasing with the $ZnCl_2$/NaAc molar ratio, corresponding to diverse Zn^{2+} solvation configurations. The peak slightly shifts with the $ZnCl_2$ concentration from 278 cm^{-1} in $x = 0.2$ to 285 cm^{-1} in $x = 0.8$. While in sat. $ZnCl_2$, the peak blue shifts about 10 cm^{-1} with the appearance of a shoulder at 329 cm^{-1} and a new peak at 237 cm^{-1}. Sat. $ZnCl_2$ was previously studied and the observed three peaks were assigned to $ZnCl_4^{2-}$, $Zn(H_2O)_2Cl_4^{2-}$ and ZnCl oligomers, respectively.[12,22,31] The low water content in sat. $ZnCl_2$ renders the Zn^{2+} solvation shell incomplete, bringing Cl^- close to Zn^{2+} and allowing the formation of $ZnCl_4^{2-}$ and Zn–Cl polynuclear aggregates.[17] Despite the high salt concentration in $ZnCl_2$/NaAc mixtures, there is no observation of $ZnCl_4^{2-}$ nor Zn_xCl_y oligomers. This observation could be attributed to both the decreasing concentration of $ZnCl_2$ and the potential interaction between Na^+ and Cl^- ions. Additionally, there appears to be a competition between Cl^- ions and Ac anions for positions adjacent to Zn^{2+}, further contributing to the explanation. Zhang et al.,[22] previously showed the importance of Zn—Cl interactions along with the H—bond strength in reducing the T_t in a 7.5 m $ZnCl_2$ in water. By simply adjusting the salt concentration, the T_t was lowered to −150 °C in 7.5 m concentration. Therefore, the weaker Zn–Cl interactions in our eutectic mixtures might contribute to reducing the T_t, particularly in $x = 0.4$ and $x = 0.5$ AEEs. Figure 2b,c represent the peak associated to Ac anion. The

Raman spectrum of sat. NaAc features several peaks assigned to Ac anion: in-plane O—C—O rocking vibration (480–510 cm^{-1}), O—C—O bending (600–680 cm^{-1}), C—C symmetric stretching (850–1000 cm^{-1}), H—C-H bending (1335 cm^{-1}), C═O stretching (1360–1450 cm^{-1}), and C—H stretching (2936 cm^{-1}).[32–36] The position of these peaks was all altered with the $ZnCl_2$ addition to NaAc, except C—H stretching at 2936 cm^{-1}, which remains at the same position. The in-plane O—C—O rocking vibration observed at 472 cm^{-1} in sat. NaAc was completely blue shifted to 505 cm^{-1} upon the increase of $ZnCl_2$ concentration. The peak at 472 cm^{-1} was previously assigned to free Ac anion, however, the presence of Zn^{2+} causes the peak to shift to higher frequencies.[34,35] The disappearance of the initial peak suggests that there is no free Ac present due to the formation of Zn^{2+}-Ac interactions. In the COO bending region, the peaks at 623 and 653 cm^{-1} in sat. NaAc are assigned to out-of-plane COO rocking and COO symmetric deformation, respectively. While, the 623 cm^{-1} slightly red shifts with the addition of $ZnCl_2$, the peak at 653 cm^{-1} keeps decreasing and then completely disappears in the $x = 0.5$ ratio. Moreover, a new peak popped-up at 678 cm^{-1} in $x = 0.2$ which blue shifts with $ZnCl_2$ concentration. The position of these two bands, in COO bending region, in the presence of $ZnCl_2$ is very similar to previously reported aqueous solution of $Zn(Ac)_2$.[34,35] This observation indicates the preference of Ac to coordinate to Zn^{2+} rather than Na^+, as suggested previously by Oliveira et al.[36] This can be confirmed by the blue shift of both C═O stretching (1360–1450 cm^{-1}) and C—C stretching (850–1000 cm^{-1}) vibrations in the presence of $ZnCl_2$. At a certain concentration, the peaks are split by two suggesting simultaneous coordination of Ac to Na^+ and Zn^{2+}. Therefore, the peaks at high frequencies are assigned to Zn^{2+}-Ac.

In Figure 2d, the O—H stretching vibration modes of water molecules (3000–3700 cm^{-1}) in pure water show the typical wide peak consisting of several components, which are attributed to various water molecules with different hydrogen-bonding environments in water clusters.[37] The sat. NaAc spectrum shows similar broad Raman band, suggesting the presence of water clusters that are not participating in the solvation of Na^+ or Ac^-. However, with the addition of $ZnCl_2$, the peak narrowed and blue shifted, particularly in $x = 0.4$, 0.5, and 0.6 electrolytes. These latter electrolytes feature almost one single peak at 3508 cm^{-1}, a shift of 51 cm^{-1}, indicating that the abundance of water clusters is significantly diminished in this extreme-state saline liquid (see Figure S2a, Supporting Information). To quantify furthermore the activity of water, peak deconvolution was performed in the region of 2800–3400 cm^{-1}. The different H—bond interactions in pure water were previously studied and assigned; the broad peak was deconvoluted into different components assigned to donor (D) acceptor (A), DDA, DAA, DDAA, and free water (Figure S2b, Supporting Information). DDAA means that one water molecule simultaneously donates two hydrogen atoms and accepts two hydrogen atoms with its two lone pairs of electrons. The latter corresponds to the more hydrogen-bonded water molecules with a DDAA environment. The other stretching peaks at a higher wavenumber above 3400 cm^{-1}, are assigned to water molecules that are not fully hydrogen-bonded, e.g., with DA and DDA environments.[17,38] Regarding the electrolytes, all of them show three peaks but at different positions depending on composition and water concentration. Electrolytes with $x = 0.2$ and $x = 0.4$ AEE have almost similar three water population peaks as sat. NaAc. There are two peaks at 3273 and 3459 cm^{-1}, while the third peak is red shifting from 3560 cm^{-1} in sat. NaAc to 3546 cm^{-1} in $x = 0.4$ AEE (Figures S3 and S4, Supporting Information). The latter suggests the decrease of free water with the increase of salt concentration. However, with increasing $ZnCl_2$ concentration from $x = 0.5$ AEE, different water populations are observed around 3284, 3392, and 3502 ± 6 cm^{-1} (Figure 2e; Figure S3, Supporting Information). The peak at ≈3502 ± 6 cm^{-1} represents strongly coordinated water molecules as previously reported in highly concentrated aqueous electrolytes.[12,37,39] Notably, the peak area of the strongly coordinated water ≈3502 ± 6 cm^{-1} in $x = 0.5$ AEE and $x = 0.6$ electrolytes is higher than in sat. $ZnCl_2$ (see Figure 2f).

Despite the same water coordination number of 6 with Zn^{2+} and Na^+, the activity of water is lower in the dual composition. Surprisingly, this finding shows the possibility of reducing free water without the need to increase the salt concentration. These results can be interpreted by the donor-acceptor balanced H-bonding from the simultaneous interaction of water molecule to Zn^{2+} and Ac anion. The interaction of Ac to water adjacent to Zn^{2+} in the first solvation shell shortens the O—H elongation bond- thus reducing the acidity of the proton. Yang et al., observed the same behaviour in the gel-like electrolyte composed of $ZnCl_2$ with ZnAc.[21] Indeed the amphoteric character of water results in a strongly bound water to both Zn^{2+} and Ac. Therefore, balancing donor-acceptor manipulation can be the strategy for the future preparation of high-voltage aqueous electrolytes.

2.3. Electrochemical Performance

The effect of NaAc on the electrolyte electrochemical properties was assessed by means of linear sweep voltammetry (LSV), cyclic voltammetry (CV) and galvanostatic cycling (GC). In the following, three $(ZnCl_2)_x(NaAc)_{1-x}/(H_2O)_n$ mixtures were selected (x = 0.2, 0.5, and 0.8) and compared with sat. NaAc and sat. $ZnCl_2$.

LSV was performed in order to investigate the relationship between the salt ratio and the ESW. **Figure 3a** shows the LSV results on glassy carbon electrode at a very low scanning rate of 0.2 $mV{\cdot}s^{-1}$. In comparison to the sat. $ZnCl_2$, the sat. $ZnCl_2$/NaAc mixtures show a clear increase in the electrochemical stability particularly at negative potentials. The presence of Ac anion pushes the HER from −0.5 V versus SHE in sat. $ZnCl_2$ to −0.92 V versus SHE in $x = 0.2$. The sat. NaAc shows a much higher stability at −1.17 V versus SHE. The latter data quantify the suppression of the HER in the presence of high salts, while the other data sets are of course limited by the reduction of Zn^{2+}. Even for this elemental reaction, the ligation shell and hypersaline media can stabilize Zn^{2+} by no less than 0.4 V, with concentration effects not considered. However, at positive potentials, the ESW is not affected so much by the electrolyte composition and concentration. $ZnCl_2$/NaAc mixtures with higher $ZnCl_2$ concentrations such as $x = 0.5$ AEE and $x = 0.8$ show a slight improvement in the ESW of ≈0.13 V at the positive potentials. This does not reflect the lower free water content as observed by Raman spectroscopy but rather points to chlorine reactions limiting the window at the oxidative side. The reversibility of Zn plating/stripping in various electrolytes was first investigated by CV on a Cu electrode in

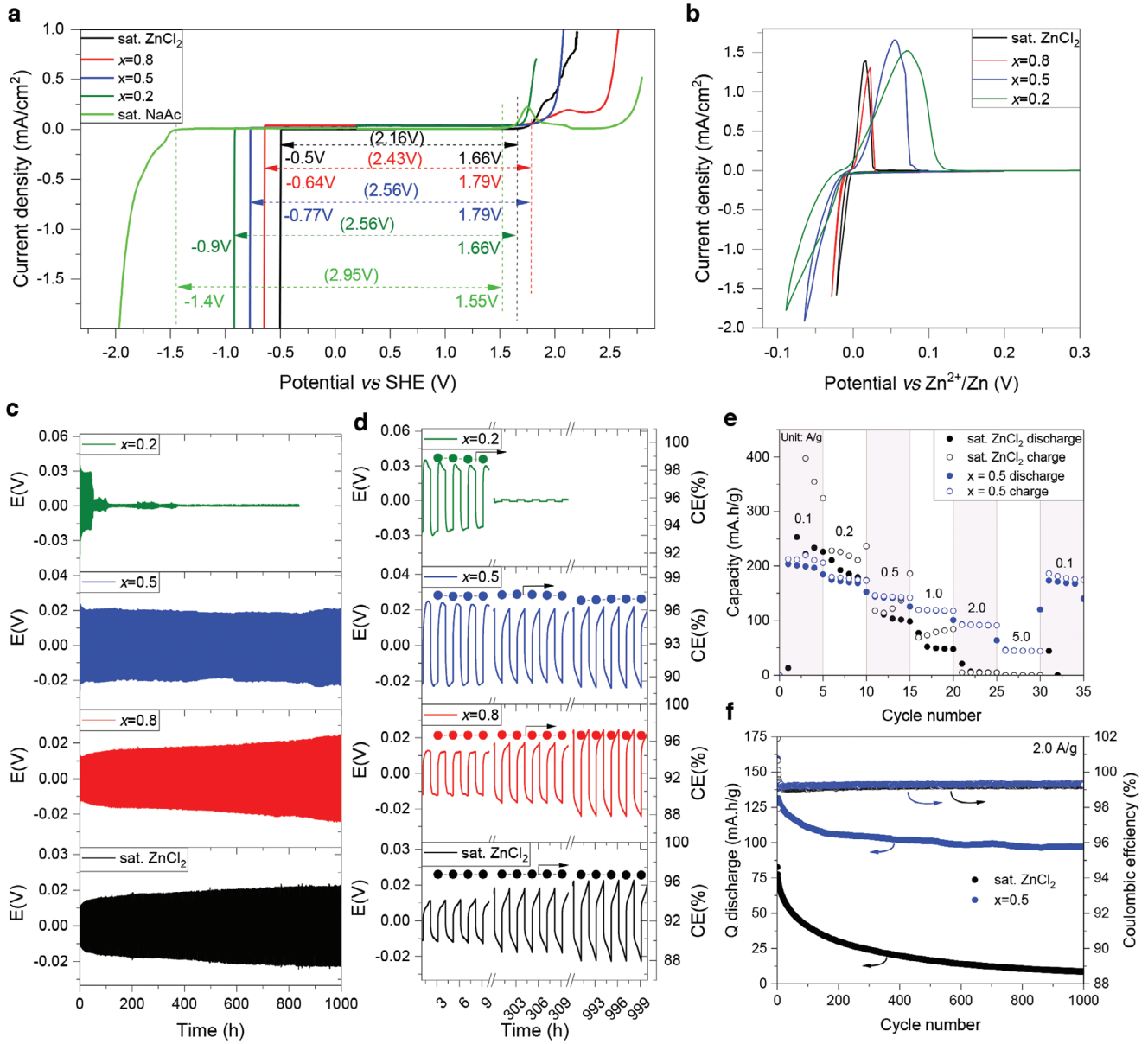

Figure 3. Electrochemical performance of $ZnCl_2$/NaAc mixtures. a) ESW on glassy carbon electrode at 0.2 mV·s^{-1} scanning rate. b) CV curves of asymmetric Zn‖Cu at 0.1 mV·s^{-1}. c,d) The cycling performance of symmetric Zn‖Zn cell at a current density of 0.2 mA·cm^{-2} and areal capacity of 0.2 mAh·cm^{-2}. e) rate capability of NaVO in full cell configuration sat. $ZnCl_2$ and $x = 0.5$ AEE. f) Long cycling stability of Zn‖NaVO full cell in sat. $ZnCl_2$ and $x = 0.5$ AEE at 2A·g^{-1} for 1000 cycles.

a symmetric Cu ‖ Zn cell (Figure 3b). The CV in the $ZnCl_2$/NaAc mixtures show a different pattern in sat. $ZnCl_2$. The CV curves become broader with increasing NaAc concentration suggesting a slower reaction kinetics. Despite $x = 0.2$ having a lower total salt concentration, the observed CV shows a higher overpotential of 0.1 V. Second, GC was performed in a symmetrical cell of Zn ‖ Zn at a current density of 0.2 mA·cm^{-2} with 2 h for each cycle (the equivalent of 0.2 mAh·cm^{-2} areal capacity). The results in Figure 3c,d demonstrate a stable response over 1000 h for sat. $ZnCl_2$ and electrolytes ratio of $x = 0.8$ and $x = 0.5$. However, the higher NaAc content in $x = 0.2$ electrolyte ratio failed after 45 h only. The Zn plating/stripping was obtained close to 0 V versus Zn/Zn^{2+}: 0.04 V versus Zn/Zn^{2+} for both $x = 0.5$ AEE and $x = 0.8$, which is similar to sat. $ZnCl_2$. However, sat. $ZnCl_2$ and $x = 0.8$ feature a lower overpotential in the first cycles around 0.02 V which increases to 0.04 V after 500 h. In contrast to $x = 0.5$ AEE which shows stable overpotential over cycling. On the other hand, the Coulombic efficiency (CE) of $x = 0.2$ and $x = 0.5$ AEE is similar to sat. $ZnCl_2$ which is 97%, with $x = 0.8$ electrolyte showing a slightly higher CE of 99% (Figure 3d). These results indicate that higher Zn ion concentration leads to better cycling stability, which can be attributed to a higher transference number ($t_{Zn^{2+}}$)(see Figure S5, Supporting Information). The obtained $t_{Zn^{2+}}$ are 0.36, 0.54, 0.48, 0.56 for $x = 0.2$, 0.5, 0.8, and sat. $ZnCl_2$

respectively. The observed high $t_{Zn^{2+}}$ in $x = 0.5$ AEE is similar to sat. $ZnCl_2$ can be attributed to the higher ionicity in the $x = 0.5$ AEE which facilitates the Zn^{2+} conductivity. Rate capability was performed for $x = 0.5$ AEE compared to sat. $ZnCl_2$ using two different areal capacities of 0.2 and 0.4 mAh·cm^{-2} as shown in Figure S6 (Supporting Information). The overpotential in $x = 0.5$ AEE is still lower than 0.1 V even at high current densities such as 3 and 5 mA·cm^{-2}. However, sat. $ZnCl_2$ exhibits a lower overpotential of less than 0.06 V at 5 mA cm^{-2}, which is expected given that the Zn content is higher than for $x = 0.5$ AEE. However, the sat. $ZnCl_2$ features a higher polarization in the voltage profile for both areal capacities (zoomed-in insets in Figure S6, Supporting Information), while $x = 0.5$ AEE demonstrates a rather flat potential. Figure S7a (Supporting Information). shows a comparison of sat. $ZnCl_2$ and $x = 0.5$ electrolyte when 1 mA·cm^{-2} rate in which both electrolytes show an overpotential of less than 0.05 V, however, the sat. $ZnCl_2$ shows polarisation after the first 100 cycles (Figure S7b, Supporting Information) while the $x = 0.5$ shows stable cycling throughout the experiment. Overall, the 0.5 AEE shows stable cycling with a low overpotential of 0.04 V in comparison with the other reported hybrid Zn electrolytes which are usually above 0.1 V versus Zn/Zn^{2+}. The latter might be explained by lower polarization, good ionic conductivity, and the absence of parasitic coating layers from side products. Afterwards, the Zn metal was recovered for surface analysis, however, the usage of a glass fibre separator promotes the plating within the separator pores making it impossible to study the surface of the Zn electrode.

Full battery cells using sodium vanadium oxide $NaV_3O_8 \cdot 1.5H_2O$ (NaVO) as a cathode and Zn metal anode were prepared and tested in sat. $ZnCl_2$ and $x = 0.5$ AEE. NaVO was obtained through a facile liquid–solid stirring method following the synthesis procedure reported by Wan et al.[40] (see Supporting Information for more details). The crystal structure and morphology of NaVO were confirmed by X-ray diffraction (XRD) and Scanning electron microscopy (SEM) (Figure S8a,b, Supporting Information).[40] Energy dispersive X-ray (EDX) results indicate the homogenous distribution of the elements Na, V, and O as shown in Figure S8c,d. The rate capability ranging from 0.1 to 5A·g^{-1} and the CE values can be found in the Figure 3e and Figure S9 (Supporting Information), respectively. NaVO cathode displays unstable cycling with poor CE in sat. $ZnCl_2$, as demonstrated by the potential profiles in Figure S10b (Supporting Information). A plateau around 0.65 V is observed at a low current density of 0.1 A·g^{-1}, reaching a high capacity of over 900 mAh·g^{-1}. The latter points to electrolyte decomposition, which is most likely driven by Cl^- oxidation. As for $x = 0.5$ AEE, NaVO cycling is more stable with better rate capability, higher CE of 90–99.7%, and good capacity recovery. The improved behaviour can be related to the wider electrochemical stability of $x = 0.5$ AEE observed in the LSV results. Long cycling stability at 2 A·g^{-1} is presented in Figure 3f and Figure S11 (Supporting Information) and show an improvement of both capacity and cycling stability in $x = 0.5$ AEE. The latter shows a higher capacity of 130 mAh·g^{-1} and capacity retention of 77% after 500, and 74% after 1000 cycles. In contrast to sat. $ZnCl_2$ which displays a first capacity of 80 mAh·g^{-1} but only 10% capacity retention after 1000 cycles. Additionally, our results are comparable to those reported by Jo et.al. using the same cathode NaVO in fluorinated 1 M $Zn(OTf)_2$ aqueous electrolyte – demonstrating a capacity retention of 82% at 3.5 A·g^{-1} for 500 cycles[41] These findings demonstrate the AEE's superior cycling stability when compared to standard $ZnCl_2$.

2.4. Compatibility Towards Al Current Collector

Al is the most used current collector in batteries mainly because of its low price and good electric conductivity. However, Al exhibits challenging corrosion in most electrolytes, particularly non-aqueous ones, which constitutes a significant focus of ongoing research in the battery field.[42] In general, it is widely accepted that the corrosion rate is proportional to the acidity of the solution, implying that the rate decreases with increasing pH.[18] Therefore, the higher pH values of the $ZnCl_2$/NaAc mixtures should reduce the corrosion of the Al current collector. $x = 0.2$, 0.5, and 0.8 electrolytes were selected to study the effect of NaAc concentration on Al corrosion. First, an electrochemical corrosion test was performed on Al in a three-electrode cell. The results exhibit a higher corrosion potentials upon the addition of NaAc except for $x = 0.8$ which shows slightly lower corrosion potential than sat. $ZnCl_2$ (see **Figure 4a**). The results are in agreement with the pH solution value as $x = 0.8$ still exhibits a low pH of 3. Furthermore, $x = 0.8$ has a total salt concentration of 16m while also having a high $ZnCl_2$ ratio, which may explain the increase in corrosion attack. Furthermore, to assess the stability of Al foil in the $ZnCl_2$/NaAc mixtures, an immersion test was performed by putting small pieces of Al foil, without previous corrosion protection, in contact with the electrolytes. The corrosion behaviour was assessed visually as pictured in Figure 4b. A visible corrosion attack was observed on Al only in $x = 0.8$ after 24 h. The corrosion was then accelerated after 1 week with $x = 0.8$ and sat. $ZnCl_2$. Al in contact with $x = 0.8$ was completely dissolved by the electrolyte after 30 days while Al foils in $x = 0.5$ AEE and $x = 0.2$ show an intact surface. Furthermore, these results are in accordance with the electrochemical corrosion test. The samples were recovered after different times (1, 7, and 30 days) cleaned with distilled water and dried in a vacuum oven at 60 °C. SEM was employed to reveal localized corrosion and the evolution of the microstructure of the surface. Figure S12 (Supporting Information) shows the recovered Al foil after 1 day at different magnifications compared with a fresh sample. The pristine sample exhibits some small pits visible at higher magnification. The samples immersed in electrolytes with higher NaAc concentration sat. NaAc, $x = 0.2$ and $x = 0.5$ AEE show similar results with micrometric pitting visible only at higher magnification. Sat. $ZnCl_2$ also exhibit similar results while $x = 0.8$ indicates a clear corrosion attack. The samples after 1 week are shown in Figure S13 (Supporting Information) and exhibits increased corrosion in both $x = 0.8$ and sat. $ZnCl_2$ while no change was observed with sat. NaAc and $x = 0.5$ AEE. The sample at $x = 0.2$ indicates small corrosion and formation of some particles. Again, after 1 month, the Al foils in contact with sat. NaAc and $x = 0.5$ AEE indicate a smooth surface at lower magnification, small pitting can be observed at higher magnification similar to the ones after 1 day. While the sample at $x = 0.2$ indicates slightly better results than after 1 week, Al foil with sat. $ZnCl_2$ indicates a clear corrosion attack with a rough surface. Overall, the

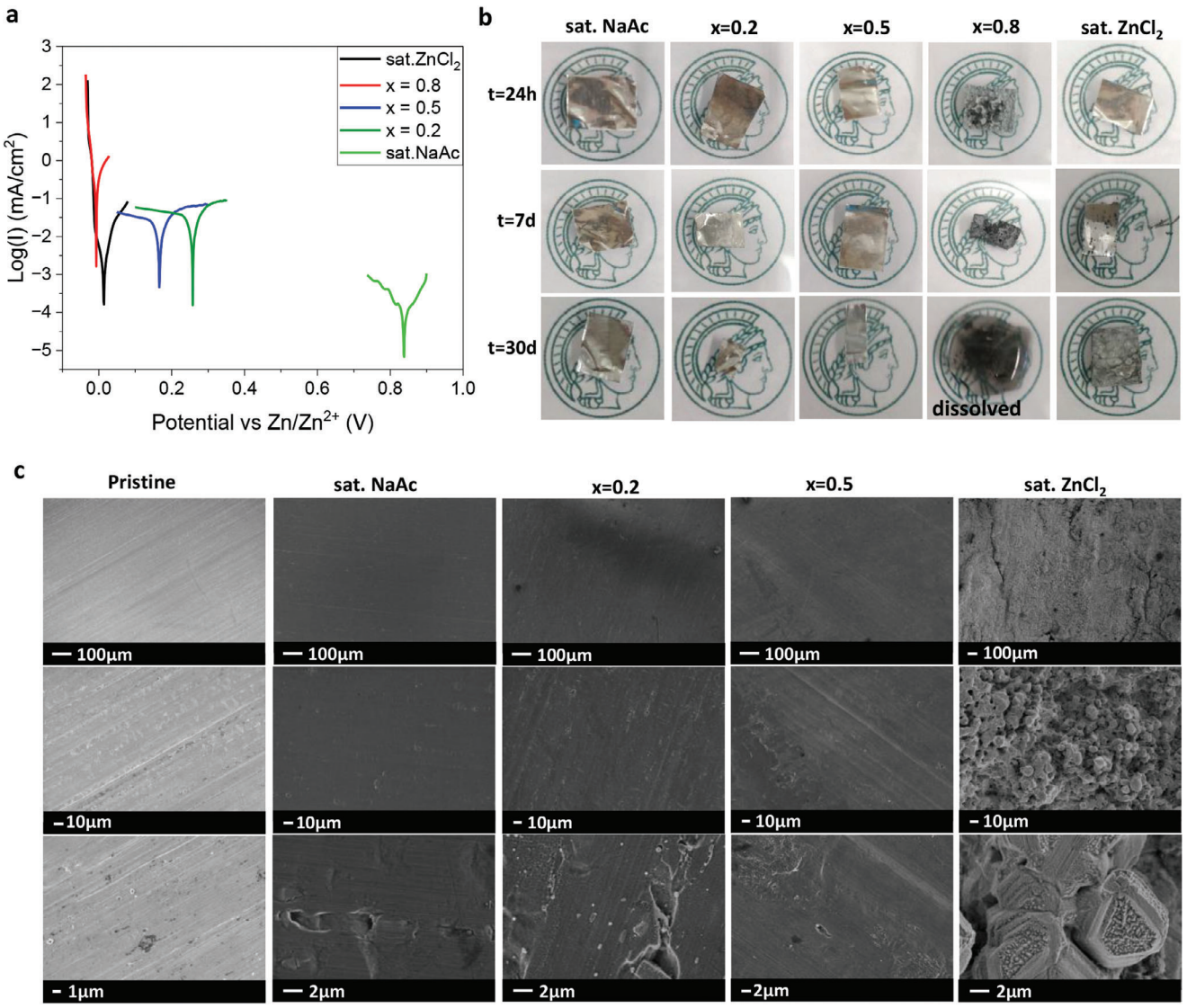

Figure 4. Corrosion tests of AEE on Al foil. a) electrochemical corrosion test on Al foil. b) visual observation of Al corrosion in contact with $x = 0$, 0.2, 0.5, 0.8, and 1 electrolytes. c) SEM images of the recovered Al foils after 30 days at three different magnifications.

results indicate that AEE $x = 0.5$ shows similar results than sat. NaAc with a slight local corrosion which doesn't increase with time.

An open environment corrosion test was also performed by simply putting a drop of electrolytes on the surface of Al foil (see Figure S14a, Supporting Information). The pictures show similar results, a visual corrosion with sat. $ZnCl_2$ and $x = 0.8$. The SEM images of recovered Al in Figure S14b (Supporting Information), indicate that electrolytes with higher NaAc concentration and sat. NaAc improve corrosion resistance. The $x = 0.5$ AEE exhibits small pits at higher magnification very close to the topography of the pristine sample. The corrosion of sat. $ZnCl_2$ is higher in an open environment and this might be explained by the hygroscopic effect of $ZnCl_2$ which adsorbs water and increases the corrosion rate. Overall, Al stability is greatly improved in $x = 0.5$ AEE compared to sat. $ZnCl_2$ and additional Al surface protection will improve its stability even further.

2.5. Improved Cellulose Separator Stability by AEE

The importance of $ZnCl_2$ concentration in dissolving cellulose was reported before.[17,43] In saturated solutions, the Lewis acidity of Zn^{2+} makes the system a strong hydrogen donor and further makes $ZnCl_4^{2-}$ a weak hydrogen bond acceptor, excellent conditions for cellulose dissolution. Sen et al., showed that cellulose solubility occurs via coordination of the primary OH to the hydrated Zn cation with some ring hydroxyls forming part of a second coordination shell around the cation. In this work, the presence of Ac increases the pH by participating in the Zn^{2+} cation solvation shell, making the system only a weaker hydrogen donor.

We, therefore, investigated the cellulose separator's stability in the $x = 0.5$ AEE. Ex situ studies were performed by putting the cellulose separator in contact with the $ZnCl_2$/NaAc mixtures as well as sat. $ZnCl_2$ and sat. NaAc. The separators were recovered after 24 h and washed thoroughly with deionized water

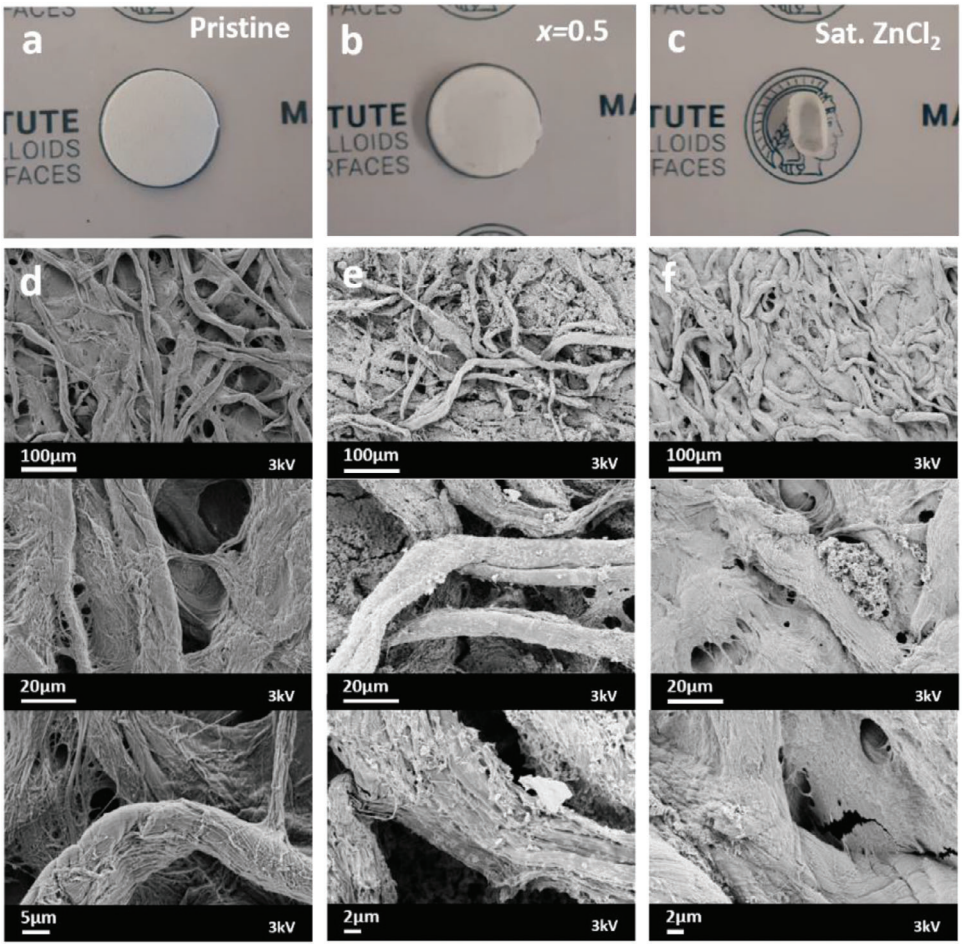

Figure 5. Cellulose separator stability after Zn‖Zn cells cycling in $x = 0.5$ AEE and sat. $ZnCl_2$ electrolytes. a–c) Visual observation of pristine cellulose and cellulose in contact with $x = 0.5$ AEE and sat. $ZnCl_2$, respectively. d–f) SEM images, at three different magnifications, of pristine cellulose and cellulose recovered in $x = 0.5$ AEE and sat. $ZnCl_2$ electrolytes, respectively.

followed by overnight drying at 50 °C (see Figure S15, Supporting Information). The effect of sat. $ZnCl_2$ electrolyte on cellulose was already visually spectacular; the separator was swollen and then completely shrunk after drying. In contrast, the cellulose separator kept shape with the rest of the electrolytes. SEM analysis was used to characterize the cellulose surface structure. The native cellulose (Figure S16, Supporting Information) exhibits a porous and fibre-like structure composed of very thin fibres. In contrast, the cellulose in contact with sat. $ZnCl_2$ reveals quite a dense structure with almost disappeared fibres. All other electrolytes, $x = 0.2$, 0.5, and 0.8 and sat. NaAc display almost no change in comparison to the reference sample and a similar fibre structure to native cellulose.

Galvanostatic cycling in Zn‖Zn cells was performed to study the cellulose stability in the previously selected electrolyte $x = 0.5$ AEE compared to sat. $ZnCl_2$ (see Figure S17, Supporting Information). The separators were recovered after 100 cycles, equivalent to 207 h, followed by washing and overnight drying at 50 °C. Compared with the pristine cellulose, the separator in $x = 0.5$ AEE displaced an unchanged shape and colour, as pictured in **Figure** 5a,b. Again, cellulose in sat. $ZnCl_2$ was swollen and completely shrunk after washing and drying (see Figure 5c). SEM images revealed almost the same results as ex situ studies but small particle precipitation can be observed on the upper fibres. The particles might be precipitated salt or ZnO reaction products. Overall, the separator in $x = 0.5$ AEE shows to keep the fibre structure of the cellulose as pictured in Figures 5d,e. These results confirm the stability of the cellulose separator in the eutectic electrolytes.

Finally, unlike the glass fibre separator, the Zn metal anode can be easily recovered from the cellulose separator. The SEM images in Figure S18 (Supporting Information) show a formation of dendrites in sat. $ZnCl_2$ while a smooth bump like can be observed in $x = 0.5$. The AEE suppresses the dendrite formation in comparison to sat. $ZnCl_2$. These results further confirm the suppression of HER in the $x = 0.5$ AEE. Furthermore, X-ray photoelectron spectroscopy (XPS) analysis was conducted to study the chemical composition of the interface after cycling. The Figure S19 (Supporting Information) shows a deposition in both sat. $ZnCl_2$ and $x = 0.5$ AEE in comparison to the pristine electrode. A similar chemical composition is seen, except the peak at 290 eV, attributed to carbonates (O—C═O), showing a higher intensity in $x = 0.5$ related to Ac anion decomposition. $ZnCl_2$ can be found at 198.8 and 200.5 while metal oxides such as ZnOH at 530.33.

Additionally, Na is found at 1072 eV, and it also contributes to 530.2 eV as NaO_2.[44] The results show that the presence of NaAc has little effect on the chemical composition of the Zn anode, except for the presence of Na, which indicates its contribution to Zn anode stabilization. The presence of Na^+, which has a lower redox potential, may act as an electrostatic shield to prevent the formation of dendrites as shown by Wan et al.[40] These findings demonstrate the numerous benefits of NaAc in eutectic electrolytes.

3. Conclusion

By simply balancing the H-bonding in the aqueous $ZnCl_2$ and NaAc mixture, an AEE with unique properties is reported. Raman spectroscopy revealed a new Zn solvation shell structure in the presence of Ac anion. At a ratio close to 0.5, both Ac and Cl^- compete with water molecules to solvate the Zn cation. Furthermore, the narrowed and blue-shifted H_2O Raman band at about 3508 cm^{-1}, indicates strong water coordination. Surprisingly, the free water population was reduced even at a lower salt concentration of 18.5 m compared to ≈31 m $ZnCl_2$. The $x = 0.5$ AEE features high transport properties also indicated by low glass transition of −77 °C. Most importantly, the ESW was broadened particularly on the negative, reductive side, thus effectively suppressing HER. High Zn plating/stripping reversibility was obtained with a low polarization voltage of only 0.04 V. Moreover, the optimised ratio at $x = 0.5$ AEE shows an improved cycling stability of NaVO cathode with a capacity retention of 74% after 1000 cycles and 99% CE. Furthermore, the presence of Ac anion in the Zn solvation shell brings a well donor–acceptor balanced H-bonding, which results in higher pH of the solution. This simple strategy allows impressive improvement of Al current collector stability as well as cellulose separator in $x = 0.5$ AEE. This work, which makes use of abundant, inexpensive, and easily up-scalable salts, provides an effective strategy for future industrial implementation of AZB.

Supporting Information

Supporting Information is available from the Wiley Online Library or from the author.

Acknowledgements

This project has received funding from the European Union's Framework Program for Research and Innovation Horizon 2020 (2014-2021) under the Marie Skłodowska-Curie Grant Agreement No. 101032227.

Open access funding enabled and organized by Projekt DEAL.

Conflict of Interest

The authors declare no conflict of interest.

Data Availability Statement

The data that support the findings of this study are available from the corresponding author upon reasonable request.

Keywords

aqueous eutectic electrolyte, aqueous Zinc batteries, transport properties, water coordination

Received: October 21, 2023
Published online: December 3, 2023

[1] Y. Shi, Y. Chen, L. Shi, K. Wang, B. Wang, L. Li, Y. Ma, Y. Li, Z. Sun, W. Ali, S. Ding, *Small* **2020**, *16*, 2000730.
[2] G. Fang, J. Zhou, A. Pan, S. Liang, *ACS Energy Lett.* **2018**, *3*, 2480.
[3] J. Yang, B. Yin, Y. Sun, H. Pan, W. Sun, B. Jia, S. Zhang, T. Ma, *Nano-Micro Lett.* **2022**, *14*.
[4] D. Kundu, B. D. Adams, V. Duffort, S. H. Vajargah, L. F. Nazar, *Nat. Energy* **2016**, *1*, 1.
[5] H. Dong, J. Li, J. Guo, F. Lai, F. Zhao, Y. Jiao, D. J. L. Brett, T. Liu, G. He, I. P. Parkin, *Adv. Mater.* **2021**, *33*, 2007548.
[6] D. Han, C. Cui, K. Zhang, Z. Wang, J. Gao, Y. Guo, Z. Zhang, S. Wu, L. Yin, Z. Weng, F. Kang, Q.-H. Yang, *Nat. Sustain.* **2021**, *5*, 205.
[7] Q. Yang, G. Liang, Y. Guo, Z. Liu, B. Yan, D. Wang, Z. Huang, X. Li, J. Fan, C. Zhi, *Adv. Mater.* **2019**, *31*, 1903778.
[8] H. Yan, X. Zhang, Z. Yang, M. Xia, C. Xu, Y. Liu, H. Yu, L. Zhang, J. Shu, *Coord. Chem. Rev.* **2022**, *452*, 214297.
[9] F. Wang, O. Borodin, T. Gao, X. Fan, W. Sun, F. Han, A. Faraone, J. A. Dura, K. Xu, C. Wang, *Nat. Mater.* **2018**, *17*, 543.
[10] R. Demir-Cakan, M. R. Palacin, L. Croguennec, *J. Mater. Chem. A* **2019**, *7*, 20519.
[11] Z. Yi, G. Chen, F. Hou, L. Wang, J. Liang, *Adv. Energy Mater.* **2021**, *11*, 2003065.
[12] C. Zhang, J. Holoubek, X. Wu, A. Daniyar, L. Zhu, C. Chen, D. P. Leonard, I. A. Rodríguez-Pérez, J.-X. Jiang, C. Fang, X. Ji, *Chem. Commun.* **2018**, *54*, 14097.
[13] C. Yang, J. Xia, C. Cui, T. P. Pollard, J. Vatamanu, A. Faraone, J. A. Dura, M. Tyagi, A. Kattan, E. Thimsen, J. Xu, W. Song, E. Hu, X. Ji, S. Hou, X. Zhang, M. S. Ding, S. Hwang, D. Su, Y. Ren, X.-Q. Yang, H. Wang, O. Borodin, C. Wang, *Nat. Sustain.* **2023**, *6*, 325.
[14] C. Zhang, W. Shin, L. Zhu, C. Chen, J. C. Neuefeind, Y. Xu, S. I. Allec, C. Liu, Z. Wei, A. Daniyar, J.-X. Jiang, C. Fang, P. Alex Greaney, X. Ji, *Carbon Energy* **2021**, *3*, 339.
[15] H. Jiang, L. Tang, Y. Fu, S. Wang, S. K. Sandstrom, A. M. Scida, G. Li, D. Hoang, J. J. Hong, N.-C. Chiu, K. C. Stylianou, W. F. Stickle, D. Wang, J. Li, P. A. Greaney, C. Fang, X. Ji, *Nat. Sustain.* **2023**, *6*, 806.
[16] L. Zhang, I. A. Rodríguez-Pérez, H. Jiang, C. Zhang, D. P. Leonard, Q. Guo, W. Wang, S. Han, L. Wang, X. Ji, *Adv. Funct. Mater.* **2019**, *29*, 1902653.
[17] X. Ji, *eScience* **2021**, *1*, 99.
[18] S. Sen, B. P. Losey, E. E. Gordon, D. S. Argyropoulos, J. D. Martin, *J. Phys. Chem. B* **2016**, *120*, 1134.
[19] J. Xiong, J. Ye, X. F. Zhao, *Kyushu Kogyo Daigaku Kenkyu Hokoku, Kogaku* **2010**, *38*, 23.
[20] A. P. Abbott, S. S. M. Alabdullah, A. Y. M. Al-Murshedi, K. S. Ryder, *Faraday Discuss.* **2018**, *206*, 365.
[21] M. Yang, J. Zhu, S. Bi, R. Wang, Z. Niu, *Adv. Mater.* **2022**, *34*, 2201744.
[22] Q. Zhang, Y. Ma, Y. Lu, L. Li, F. Wan, K. Zhang, J. Chen, *Nat. Commun.* **2020**, *11*, 4463.
[23] X. Jin, M. A. Medina, X. Zhang, S. Zhang, *Int. J. Thermophys.* **2014**, *35*, 45.
[24] D. I. Iermakova, R. Dugas, M. R. Palacín, A. Ponrouch, *J. Electrochem. Soc.* **2015**, *162*, A7060.
[25] R. Hachicha, R. Zarrougui, S. Messaoudi, S. Le Vot, O. Fontaine, F. Favier, O. Ghodbane, *J. Mol. Liq.* **2019**, *284*, 522.
[26] A. R. Neale, S. Murphy, P. Goodrich, C. Hardacre, J. Jacquemin, *ChemPhysChem* **2017**, *18*, 2040.

[27] M. S. Ding, K. Xu, *J. Phys. Chem. C* **2018**, *122*, 16624.
[28] M. S. Ding, A. Von Cresce, K. Xu, *J. Phys. Chem. C* **2017**, *121*, 2149.
[29] M. S. Ding, *J. Chem. Eng. Data* **2003**, *48*, 519.
[30] J. Han, A. Mariani, S. Passerini, A. Varzi, *Energy Environ. Sci.* **2023**, *16*, 1480.
[31] D. E. Irish, B. Mccarroll, T. F. Young, *J Chem Phys* **1963**, *39*, 3436.
[32] K. Ito, H. J. Bernstein, *Can. J. Chem.* **1956**, *34*, 170.
[33] H. Noma, Y. Miwa, I. Yokoyama, K. Machida, *J. Mol. Struct.* **1991**, *242*, 207.
[34] M. M. Yang, D. A. Crerar, D. E. Irish, *Geochim. Cosmochim. Acta* **1989**, *53*, 319.
[35] R. L. Frost, J. T. Kloprogge, *J. Mol. Struct.* **2000**, *526*, 131.
[36] D. Mendes De Oliveira, S. R. Zukowski, V. Palivec, J. Hénin, H. Martinez-Seara, D. Ben-Amotz, P. Jungwirth, E. Duboué-Dijon, *Phys. Chem. Chem. Phys.* **2020**, *22*, 24014.
[37] Y. Yamada, K. Usui, K. Sodeyama, S. Ko, Y. Tateyama, A. Yamada, *Nat. Energy* **2016**, *1*, 16129.
[38] Q. Hu, H. Zhao, S. Ouyang, *Phys. Chem. Chem. Phys.* **2017**, *19*, 21540.
[39] L. Suo, O. Borodin, T. Gao, M. Olguin, J. Ho, X. Fan, C. Luo, C. Wang, K. Xu, *Science.* **2015**, *350*, 938.
[40] F. Wan, L. Zhang, X. Dai, X. Wang, Z. Niu, J. Chen, *Nat. Commun.* **2018**, *9*, 1656.
[41] J. H. Jo, Y. Aniskevich, J. Kim, J. U. Choi, H. J. Kim, Y. H. Jung, D. Ahn, T. Y. Jeon, K. S. Lee, S. H. Song, H. Kim, G. Ragoisha, A. Mazanik, E. Streltsov, S. T. Myung, *Adv. Energy Mater.* **2020**, *10*, 2001595.
[42] S. S. Zhang, T. R. Jow, *J. Power Sources* **2002**, *109*, 458.
[43] L. Yang, G. Li, F. Yang, S.-M. Zhang, H.-X. Fan, X.-N. Lv, *Carbohydr. Res.* **2011**, *346*, 2304.
[44] Y. Zhu, J. Yin, X. Zheng, A.-H. Emwas, Y. Lei, O. F. Mohammed, Y. Cui, H. N. Alshareef, *Energy Environ. Sci* **2021**, *14*, 4463.